Stochastic Misalignment Model for Magneto-Inductive SISO and MIMO Links

Gregor Dumphart and Armin Wittneben
Communication Technology Laboratory, ETH Zurich, 8092 Zurich, Switzerland
Email: {dumphart, wittneben}@nari.ee.ethz.ch

***Abstract*—Magneto-inductive (MI) systems for wireless communications or power transfer usually suffer from coil misalignment, because of mobility or deployment. The impact on performance is hard to analyze because mutual inductance is an involved function of geometry. We focus on links whose coil separation exceeds coil dimensions, which is characteristic for communications links and becoming increasingly desired for wireless powering. In this regime, the dipole approximation allows for an accurate closed-form description of misalignment. In order to analyze fully unaligned links, we propose a stochastic misalignment model that assumes uniformly random coil orientation(s). To this effect, we derive the probability density function (PDF) of mutual inductance for practically relevant setups, comprising single coils and collocated coil arrays. This gives rise to a misalignment comparison of beamforming, coil selection, and single-input single-output (SISO) links. The PDFs lead to the expected attenuation due to misalignment. We relate misalignment to communications performance by means of a basic circuit. A byproduct of the stochastic model is the maximum likelihood range estimate for a noiseless mutual inductance measurement under unknown arrangement.**

I. Introduction

Magneto-inductive (MI) near-field links are at the basis of omnipresent RFID and NFC systems and constitute a powerful physical layer for wireless power transfer [1], [2], communications in harsh media [3], [4], medical applications [5], [6], and microsensor networks where far-field radio requires THz frequencies. In addition to the intrinsically high path loss, practical systems suffer from misalignment whenever coaxial coil arrangement cannot be enforced, e.g. for freely moving systems like in-vivo biomedical systems [5], sensors deployed in harsh environments [3], [4], or handheld RFID readers. A popular means for misalignment mitigation are coil arrays for spatial diversity [2], [4], [5].

Mutual inductance M is a key quantity for the description of misalignment and path loss: M^2 multiplies power transfer efficiency as well as squared channel gain of direct communications (as opposed to load modulation) in the weak-coupling regime [5], [6]. However, M is a complicated function of arrangement and coil geometry: for example, M between electrically small thin-wire coils is described by the Neumann formula [7], a double line integral whose evaluation requires numerical methods in general. Previous studies of misalignment (i.e. the decrease in mutual inductance due to deviation from coaxial arrangement) were mostly concerned with efficient power transfer between strongly coupled coils, which is particularly complicated because of the significance of coil geometries in that regime. For example, researchers had to resort to numerical integration [8] or measurement-based approaches [9] even for the analysis of small lateral displacements of parallel flat circular filaments. These efforts were extended to more general coil shapes and angular misalignment by [10]. The evolution of M was furthermore studied over lateral and angular offsets in [11] and for a specific beamforming setup with coil arrays in [5].

However, MI applications are often desired to support separations considerably larger than the coil dimensions, for reasons of reach and mobility [1]–[4]. This leads to operation in the weak-coupling regime, where coil geometries can be neglected. In consequence, the magnetic field at the receiver (RX) resembles a dipole field, whose simple mathematical description allows for an analytic treatment of misalignment. In this tractable domain, we choose the following approach: in order to get rid of the tedious arrangement dependencies of unaligned links, we assume random arrangement and derive a stochastic model for mutual inductance at given separation. All misalignment effects are captured by a unitless random variable $J \in [-1, 1]$. This approach is inspired by models for multipath radio channels, where communication theorists prefer a stochastic treatment of fading (e.g., Rayleigh fading) over solving Maxwell's equations for specific environments. The approach is also applicable to array techniques, namely beamforming and antenna selection, which enables a comparison of their capabilities in combating misalignment. The statistical description of J leads to a closed-form treatment of expected alignment efficiency of 1×1 links and array techniques under random geometry.

In this paper, we make the following contributions. First, we discuss the dipole-field approximation of mutual inductance and apply it to 3×3 multiple-input multiple-output (MIMO) links between orthogonal, collocated coil arrays. It is seen that, regardless of arrangement, the dominant singular value of the channel matrix is 6 dB above the others, with implications for spatial multiplexing. We discuss worst-case misalignment for antenna selection and beamforming. In the stochastic main part, we derive probability density functions (PDFs) f_J under random arrangement for 1×1 links and the aforementioned array techniques, for both homogeneous-field and dipole-field cases. The statistical moments allow for an exact comparison of expected alignment efficiency which, e.g., is $\frac{1}{6}$ for dipole-field 1×1 links and improved to $\frac{1}{2}$ by single-sided beamforming. One of the PDFs implies the

maximum likelihood (ML) range estimate for a noiseless M-measurement. We conclude by putting communications performance of misaligned MI links in perspective by means of a basic circuit model.

Notation: All vectors are column vectors in $\mathbb{R}^3$ and denoted lowercase boldface, even the magnetic field $\mathbf{b}$ against conventions in physics. All matrices are in $\mathbb{R}^{3\times3}$ and written uppercase boldface. $\mathbf{I}$ is the 3×3 identity matrix. f_J is the PDF of random variable J. For simplicity, we use the same symbol for random variable and realization, e.g. $f_J(J)$.

II. Coupling Model

Consider a transmit (TX) coil running current i_t. The generated magnetic field $\mathbf{b}\in\mathbb{R}^3$ induces a voltage $v_\mathrm{r}=j\omega M\, i_\mathrm{t}$ at an RX coil, which can be regarded as noiseless signal model for this MI link. The RX coil has orientation unit vector $\mathbf{r}$, turn number N_r, and the impinging $\mathbf{b}$ is assumed homogeneous across its surface of area S_r. The *mutual inductance*

$$M = M_\text{aligned}\cdot J\ , \tag{1}$$

where $M_\text{aligned} = N_\mathrm{r}S_\mathrm{r}\,\|\mathbf{b}_\text{ax}\|\,/\,i_\mathrm{t}$ is its maximum, coaxially aligned value at a given coil separation d. $\mathbf{b}_\text{ax}$ is the field on the TX coil axis at d. The unitless *alignment factor* (or polarization factor [3]), the central quantity of this paper, is

$$J=\frac{\mathbf{r}^\mathrm{T}\mathbf{b}}{\|\mathbf{b}_\text{ax}\|}\ ,\qquad -1\le J\le 1\ . \tag{2}$$

For a small RX coil located in the axial homogeneous field of a much larger TX coil, $\mathbf{b}=\mathbf{b}_\text{ax}$. We will call this practically important setup the *homogeneous-field case*.

However, we are also interested in MI links between coils of arbitrary size, orientation, and separation like in Figure 1.

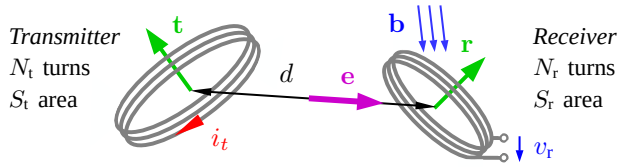

Fig. 1. Magneto-inductive 1×1 link between single coils with separation d. TX current i_t induces voltage $v_\mathrm{r}=j\omega M\, i_\mathrm{t}$ at the RX coil. Unit vector $\mathbf{e}$ points from TX to RX, while unit vectors $\mathbf{t}$ and $\mathbf{r}$ describe TX and RX coil orientations, respectively.

When d is appreciably larger than the dimensions of both coils, the influence of coil shape becomes negligible because the TX coil behaves like a magnetic dipole of dipole moment $i_\mathrm{t}N_\mathrm{t}S_\mathrm{t}\,\mathbf{t}$. By a classic formula [7, Eq 5.87], rewritten in matrix notation, the resulting $\mathbf{b}$ at RX coil location $d\mathbf{e}$ is

$$\mathbf{b} = i_\mathrm{t}\ \frac{\mu}{2\pi}\frac{N_\mathrm{t}S_\mathrm{t}}{d^3}\boldsymbol{\mathcal{E}}\mathbf{t}\ , \tag{3}$$

$$\boldsymbol{\mathcal{E}} := \tfrac{3}{2}\mathbf{e}\mathbf{e}^\mathrm{T}-\tfrac{1}{2}\mathbf{I}\ . \tag{4}$$

This leads to mutual inductance for the *dipole-field case*

$$M=\frac{K}{d^3}\,J\ , \tag{5}$$

$$J=\mathbf{r}^\mathrm{T}\boldsymbol{\mathcal{E}}\mathbf{t}\ ,\qquad -1\le J\le 1\ , \tag{6}$$

$$K=\frac{\mu}{2\pi}N_\mathrm{t}N_\mathrm{r}S_\mathrm{t}S_\mathrm{r}\ .$$

So alignment factor J accounts for the impact of three-dimensional *arrangement* $(\mathbf{e},\mathbf{t},\mathbf{r})$ on M. Permeability, turn numbers, and surface areas[1] are represented by K.

Interpretation of (6) is easiest by means of the eigenvalues of $\boldsymbol{\mathcal{E}}$: the dominant eigenvalue 1 corresponds to eigenvector $\mathbf{e}$ and *coaxial* coupling ($\mathbf{t}=\mathbf{r}=\mathbf{e}\implies J=1$), while a double eigenvalue $-\frac{1}{2}$ is associated with eigenvectors orthogonal to $\mathbf{e}$ and *coplanar* coupling ($\mathbf{t}=\mathbf{r}$ and $\mathbf{t},\mathbf{r}\perp\mathbf{e}\implies J=-\frac{1}{2}$).[2]

The notion of the dipole-field case is easily extendable to MI links involving arrays of three collocated coils. Consider the 3×3 link in Figure 2. We are interested in the mutual inductances between RX and TX coils, subsumed by 3×3 matrix $\mathbf{M}$. Coils among the same orthogonal array are uncoupled at non-radiative frequencies [12].

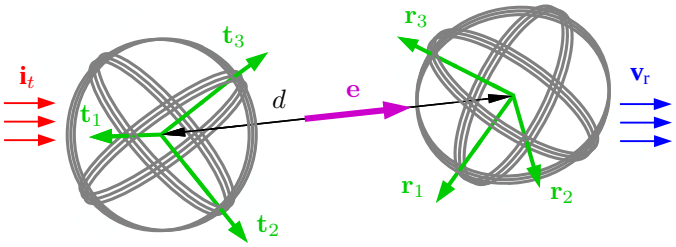

Fig. 2. Magneto-inductive 3×3 MIMO link between collocated, orthogonal coil arrays. TX current vector $\mathbf{i}$ induces voltage vector $\mathbf{v}_\mathrm{r}=j\omega\mathbf{M}\,\mathbf{i}_\mathrm{t}$ at the RX array. d and $\mathbf{e}$ are analogous to the 1×1 case due to collocation.

The induced voltages are $\mathbf{v}_\mathrm{r}=j\omega\mathbf{M}\,\mathbf{i}_\mathrm{t}$. We collect coil orientations in matrices $\mathbf{R}:=[\mathbf{r}_1,\mathbf{r}_2,\mathbf{r}_3]$ and $\mathbf{T}:=[\mathbf{t}_1,\mathbf{t}_2,\mathbf{t}_3]$ and note that d and $\mathbf{e}$ describe the separation of each coil pair. Therewith, (5) and (6) can be extended to

$$\mathbf{M}=\frac{K}{d^3}\mathbf{J}=\frac{K}{d^3}\mathbf{R}^\mathrm{T}\boldsymbol{\mathcal{E}}\mathbf{T}\ . \tag{7}$$

For any given $\mathbf{e}$ we can define an orthogonal transformation $\mathbf{U}$ (i.e. real and unitary: $\mathbf{U}^\mathrm{T}\mathbf{U}=\mathbf{U}\mathbf{U}^\mathrm{T}=\mathbf{I}$) such that $\mathbf{e}^\mathrm{T}\mathbf{U}=[1,0,0]\implies\mathbf{U}^\mathrm{T}\boldsymbol{\mathcal{E}}\mathbf{U}=\mathrm{diag}(1,-\frac{1}{2},-\frac{1}{2})$. Thus, we can consider an equivalent diagonal problem w.l.o.g.:

$$\mathbf{M}=\frac{K}{d^3}\underbrace{\mathbf{R}^\mathrm{T}\mathbf{U}}_{=:\tilde{\mathbf{R}}^\mathrm{T}}\begin{bmatrix}1&&\\&-\frac{1}{2}&\\&&-\frac{1}{2}\end{bmatrix}\underbrace{\mathbf{U}^\mathrm{T}\mathbf{T}}_{=:\tilde{\mathbf{T}}}\ . \tag{8}$$

It is evident that we can diagonalize the channel matrix $j\omega\mathbf{M}$ to $j\omega\frac{K}{d^3}\,\mathrm{diag}(1,-\frac{1}{2},-\frac{1}{2})$ with unitary TX and RX beamforming matrices $\mathbf{W}_\mathrm{t},\mathbf{W}_\mathrm{r}$ if $\tilde{\mathbf{T}},\tilde{\mathbf{R}}$ are unitary (then $\mathbf{W}_\mathrm{t}=\tilde{\mathbf{T}}^\mathrm{T}$ and $\mathbf{W}_\mathrm{r}=\tilde{\mathbf{R}}^\mathrm{T}$). This is the case for orthogonal coil arrays.

III. Specifics of MI Array Techniques

Coil arrays can be utilized with spatial multiplexing, beamforming, or antenna selection. These well-established array techniques need no further introduction. Instead, this section discusses their magneto-inductive specifics like worst-case

[1] Formulas in literature often use coil radii instead of surfaces. However, this would be an unnecessary restriction in this context: any shape (e.g. rectangular or octagonal) is eligible since the dipole model ignores coil geometry.

[2] Another prominent arrangement, of importance in NMR spectroscopy, is the magic angle case $\mathbf{e}^\mathrm{T}\mathbf{t}=1/\sqrt{3}$ while $\mathbf{t}=\mathbf{r}$, resulting in $J=0$ according to (6). Thereby, $\mathbf{b}\perp\mathbf{r}$ results in zero flux through the RX coil surface.

misalignment and establishes prerequisites for the following stochastic section.

From (8) it is clear that the described 3×3 channel can be used for **spatial multiplexing** of three parallel streams. Intuitively, this is due to the TX array steering $\mathbf{b}$ in any desired direction, resulting in three independent induced voltages at the RX array. This is a distinct feature of the near field: far-field MIMO systems, in comparison, require a rich scattering environment in order to multiplex a third stream over the magnetic field (in free space, the far field $\mathbf{b} \perp \mathbf{e}$ and thus the two orthogonal polarizations are the only spatial degrees of freedom) [13]. A rather surprising implication of (8) is that *the strongest stream has twice the amplitude of the weaker streams regardless of arrangement*, in terms of mutual inductance.

Joint optimal 3×3 beamforming uses the strongest stream in (8), which corresponds to a *coaxial* 1×1 link, i.e. $J = 1$. Optimal beamforming vectors $\mathbf{b}_\mathrm{t} = \mathbf{T}^\mathrm{T}\mathbf{e}$ and $\mathbf{b}_\mathrm{r} = \mathbf{R}^\mathrm{T}\mathbf{e}$ virtually establish a coaxial coil pair by correcting the non-coaxiality of $\mathbf{T}$ and $\mathbf{R}$. This notion of an equivalent 1×1 link of mutual inductance subject to some J is used heavily in the remainder of the paper.

By **single-sided beamforming** for the dipole-field case, we refer to either 3×1 RX-beamforming at array $\mathbf{R}$ with TX-coil $\mathbf{t}$ or 1×3 TX-beamforming from $\mathbf{T}$ to $\mathbf{r}$. The cases are analogous because of the symmetry property of mutual inductance [7]. Optimal beamforming vectors $\mathbf{b}_\mathrm{r} \propto \mathbf{R}^\mathrm{T}\mathbf{b} \propto \mathbf{R}^\mathrm{T}\boldsymbol{\mathcal{E}}\mathbf{t}$ for 3×1 or $\mathbf{b}_\mathrm{t} \propto \mathbf{T}^\mathrm{T}\boldsymbol{\mathcal{E}}\mathbf{r}$ for 1×3 follow from adaption of (7) and multi-antenna basics. To study the misalignment performance, we examine the magnitude of the 3×1 mutual inductance vector (cf. (7) and maximum-ratio combining for SIMO channels)

$$\left\| \frac{K}{d^3}\mathbf{R}^\mathrm{T}\boldsymbol{\mathcal{E}}\mathbf{t} \right\| = \frac{K}{d^3}\|\boldsymbol{\mathcal{E}}\mathbf{t}\| = \frac{K}{d^3}\,\frac{1}{2}\sqrt{1+3(\mathbf{e}^\mathrm{T}\mathbf{t})^2}\ , \qquad (9)$$

which can be obtained by using property $\boldsymbol{\mathcal{E}}^2 = \frac{1}{2}(\mathbf{I}+\boldsymbol{\mathcal{E}})$ to compute $\|\boldsymbol{\mathcal{E}}\mathbf{t}\|^2 = \mathbf{t}^\mathrm{T}\boldsymbol{\mathcal{E}}^2\mathbf{t} = \frac{1}{2} + \frac{1}{2}\mathbf{t}^\mathrm{T}\boldsymbol{\mathcal{E}}\mathbf{t} = \frac{1}{4}(1+3(\mathbf{e}^\mathrm{T}\mathbf{t})^2)$. Comparing (9) to (5) shows that optimal single-sided beamforming behaves like a 1×1 link of M subject to

$$|J| = \frac{1}{2}\sqrt{1+3a^2}\ , \quad a = \begin{cases} \mathbf{e}^\mathrm{T}\mathbf{t} & \text{for 3×1 RX Bf.} \\ \mathbf{e}^\mathrm{T}\mathbf{r} & \text{for 1×3 TX Bf.} \end{cases} . \qquad (10)$$

Therefore, $\frac{1}{2} \le |J|$ for this case. It is noteworthy that optimal TX-beamforming in general does not align $\mathbf{b}$ with $\mathbf{r}$, rather the best balance between field strength and direction is found. In the homogeneous-field case, single-sided beamforming can always achieve the optimal $|J| = 1$, which is intuitive.

In **3×3 coil selection** (cf. antenna selection), we choose the coil pair of greatest mutual inductance, or rather with the alignment factor (6) of greatest absolute value. For dipole coupling, this limits misalignment to $0.4797883 \le |J|$, which is is the greatest real root of sixth-order polynomial $(24J^3 - 8J^2 - J + 1)^2 - 16J^3$. We derive this bound and construct a worst-case arrangement in Appendix A.

A 3×1 or 1×3 channel allows for **single-sided coil selection**. Exemplarily, we analyze 3×1 worst-case misalignment (like in beamforming, 3×1 and 1×3 cases are analogous): with J in general form (2), the worst case J_wc occurs when all receive coils are at the same angle to $\mathbf{b}$, or formally

$$\frac{\mathbf{R}^\mathrm{T}\mathbf{b}}{\|\mathbf{b}_\mathrm{ax}\|} = \begin{bmatrix} \pm J_\mathrm{wc} \\ \pm J_\mathrm{wc} \\ \pm J_\mathrm{wc} \end{bmatrix} \overset{\text{magnitude}}{\Longrightarrow} \frac{\|\mathbf{b}\|}{\|\mathbf{b}_\mathrm{ax}\|} = |J_\mathrm{wc}|\sqrt{3}\ . \qquad (11)$$

For the homogeneous-field case, $\mathbf{b} = \mathbf{b}_\mathrm{ax}$ and misalignment thus limited to $\frac{1}{\sqrt{3}} \le |J|$. In the dipole-field case, on the other hand, the field-strength ratio is minimal for $\mathbf{t} \perp \mathbf{e} \implies \frac{\|\mathbf{b}\|}{\|\mathbf{b}_\mathrm{ax}\|} = \|\boldsymbol{\mathcal{E}}\mathbf{t}\| = \|-\frac{1}{2}\mathbf{t}\| = \frac{1}{2}$, imposing $\frac{1}{2\sqrt{3}} \le |J|$.

Furthermore, we consider a **3×3 hybrid technique** of (joint optimal) coil selection at one array and beamforming at the other. With exemplary RX-side coil selection, $|J| = \max_m \frac{1}{2}\sqrt{1+3a_m^2}$ with $a_m = \mathbf{e}^\mathrm{T}\mathbf{r}_m$ by (10). In the worst case, $a_m = \frac{1}{\sqrt{3}}\ \forall m$ according to (11), giving $\frac{1}{\sqrt{2}} \le |J|$.

IV. Stochastic Misalignment Analysis

We established $M = M_\mathrm{aligned} \cdot J$ and, more specifically, $M = \frac{K}{d^3}J$ in Section II, where J is a simple function of arrangement. However, we desire a model that is completely detached from specific geometries in order to analyze the performance of unaligned links. This gives rise to the idea of regarding J as a random variable instead of bothering about its actual value for a given arrangement. This section studies the statistics of J of the introduced scenarios under random arrangement. Their moments $\mathrm{E}(J^2)$ and $\mathrm{E}(J^4)$ can be regarded as *expected alignment efficiency* of direct links and load modulation (which essentially uses the inductive channel twice, cf. passive RFID), respectively. Alignment efficiency multiplies squared channel gain in the weak-coupling regime.

Definition: We say a random unit vector is of *spherical uniform distribution* when all directions are equiprobable, i.e. when the vector has uniform distribution on the unit sphere. Therewith, we model unknown or arbitrary coil orientations (e.g., think of RFID tags on stored goods or mobile nodes like a wirelessly charged cellphone in a pants pocket [2]).

Samples can be drawn by normalization $\mathbf{r} = \mathbf{g} \,/\, \|\mathbf{g}\|$ of three-dimensional Gaussian samples $\mathbf{g} \sim \mathcal{N}(\mathbf{0}, \mathbf{I})$. [14]

Homogeneous-field case, 1 × 1 link: For random $\mathbf{r}$ of spherical uniform distribution in a homogeneous magnetic field, the alignment factor has uniform distribution

$$J \sim \mathcal{U}(-1, +1) \qquad (12)$$

with moments $\mathrm{E}(J^2) = \frac{1}{3}$ and $\mathrm{E}(J^4) = \frac{1}{5}$.

Proof: With $J = \mathbf{r}^\mathrm{T}\frac{\mathbf{b}}{\|\mathbf{b}\|}$ and all directions $\mathbf{r}$ equiprobable, we note that J has the same statistics as any projection of $\mathbf{r}$. In particular, the canonical projection $r_z = [0\ 0\ 1]\mathbf{r}$ has CDF

$$\Pr(r_z \le \xi) = \iint\limits_{\|\mathbf{r}\|=1, r_z \le \xi} 1\,dS \ \Big/ \oiint\limits_{\|\mathbf{r}\|=1} 1\,dS$$
$$= \frac{A(\text{height } 1+\xi \text{ unit sph. cap})}{A(\text{full unit sphere})} = \frac{2\pi(1+\xi)}{4\pi} = \frac{1+\xi}{2}\ .$$

This CDF grows linearly in ξ between $\Pr(r_z \le -1) = 0$ and $\Pr(r_z \le 1) = 1$, so $r_z \sim \mathcal{U}(-1, 1)$ and thus $J \sim \mathcal{U}(-1, 1)$. The moments of the uniform distribution are well known. □

Dipole-field case, 1×1 link: For random $\mathbf{t}$ and $\mathbf{r}$ (or equivalently: $\mathbf{t}$ and $\mathbf{e}$ or $\mathbf{r}$ and $\mathbf{e}$) of spherical uniform distribution, the alignment factor has distribution

$$f_J(J) = \begin{cases} \frac{\operatorname{arsinh}\sqrt{3}}{\sqrt{3}} & |J| \le \frac{1}{2} \\ \frac{\operatorname{arsinh}\sqrt{3} \;-\; \operatorname{arsinh}\sqrt{4J^2-1}}{\sqrt{3}} & \frac{1}{2} < |J| \le 1 \\ 0 & 1 < |J| \end{cases} \tag{13}$$

with moments $\mathrm{E}(J^2) = \frac{1}{6}$ and $\mathrm{E}(J^4) = \frac{3}{50}$.

Proof: Let $T := \mathbf{e}^{\mathrm{T}}\mathbf{t}$ where $\mathbf{e}$ is constant and $\mathbf{t}$ random of spherical uniform distribution. Then $T \sim \mathcal{U}(-1,1)$ by the argument of (12). Equations (2) and (3) yield $\|\mathbf{b}\| \,/\, \|\mathbf{b}_{\mathrm{ax}}\| = \|\boldsymbol{\mathcal{E}}\mathbf{t}\| = \frac{1}{2}\sqrt{1+3(\mathbf{e}^{\mathrm{T}}\mathbf{t})^2} = \frac{1}{2}\sqrt{1+3T^2}$ for the dipole-field case. $\mathbf{r}$ has spherical uniform distribution in field $\mathbf{b}$, so $J = \mathbf{r}^{\mathrm{T}}\mathbf{b} \,/\, \|\mathbf{b}_{\mathrm{ax}}\|$ has uniform distribution over interval $\mathcal{J}(T) := \left[-\frac{1}{2}\sqrt{1+3T^2}, \frac{1}{2}\sqrt{1+3T^2}\right]$ given T, or rather

$$f_{J|T}(J|T) = \frac{\mathbb{1}_{\mathcal{J}(T)}(J)}{\sqrt{1+3T^2}} \; .$$

In order to obtain f_J, we marginalize the joint PDF on J, T.

$$f_J(J) = \int_{-1}^{1} f_{J|T}(J|T) f_T(T) dT = \int_0^1 \frac{\mathbb{1}_{\mathcal{J}(T)}(J)}{\sqrt{1+3T^2}} \; dT$$

For case $|J| \le \frac{1}{2}$, $J \in \mathcal{J}(T)$ holds because $[-\frac{1}{2}, \frac{1}{2}] \subseteq \mathcal{J}(T)$ for any T. Thus, for this case

$$f_J(J) = \int_0^1 \frac{dT}{\sqrt{1+3T^2}} = \frac{\operatorname{arsinh}\sqrt{3}}{\sqrt{3}} \; .$$

For case $\frac{1}{2} < |J| \le 1$, set membership $J \in \mathcal{J}(T)$ holds if $|J| \le \frac{1}{2}\sqrt{1+3T^2}$, or rather $\sqrt{4J^2-1}/\sqrt{3} \le |T|$. Therefore,

$$f_J(J) = \int_{\frac{\sqrt{4J^2-1}}{\sqrt{3}}}^{1} \frac{dT}{\sqrt{1+3T^2}} = \frac{\operatorname{arsinh}\sqrt{3} - \operatorname{arsinh}\sqrt{4J^2-1}}{\sqrt{3}} \; .$$

Case $1 < |J|$ results in $f_J(J) = 0$ because $J \notin \mathcal{J}(T)$ due to $|T| \le 1 \Longrightarrow \mathcal{J}(T) \subseteq [-1,1]$. The moments follow from integration $\mathrm{E}(J^k) = \int_{-1}^{+1} J^k f_J(J) \; dJ$, which is omitted. □

Homogeneous-field case, single-sided coil selection: With uniformly random array orientation $\mathbf{R}$ (or $\mathbf{T}$), the chosen coil pair has mutual inductance subject to

$$f_J(J) = \begin{cases} \frac{3}{2}\left(1 - \frac{4}{\pi}\arccos\frac{|J|}{\sqrt{1-J^2}}\right) & \frac{1}{\sqrt{3}} \le |J| < \frac{1}{\sqrt{2}} \\ \frac{3}{2} & \frac{1}{\sqrt{2}} \le |J| \le 1 \\ 0 & \text{otherwise} \end{cases} \tag{14}$$

with moments $\mathrm{E}(J^2) = \frac{1}{3} + \frac{2}{\pi\sqrt{3}}$ and $\mathrm{E}(J^4) = \frac{1}{5} + \frac{26}{15\pi\sqrt{3}}$.

Proof: The 3×1 setup in Figure 3 guides the proof. Let $J_m = \mathbf{r}_m^{\mathrm{T}} \frac{\mathbf{b}}{\|\mathbf{b}\|}$. We denote E_m for the event that $|J_m|$ is largest. $\Pr(E_m \;|\; \frac{1}{\sqrt{2}} < |J_m|) = 1$ follows from the sketch while $\Pr(E_m \;|\; |J_m| < \frac{1}{\sqrt{3}}) = 0$ is due to (11). When $\mathbf{r}_1$ is fixed, the angles of $\mathbf{r}_2$ and $\mathbf{r}_3$ on their orthogonal plane have uniform distribution. E_1 does not occur when any of $\mathbf{r}_2, \mathbf{r}_3, -\mathbf{r}_2, -\mathbf{r}_3$ is in the red sector of angle α, and therefore

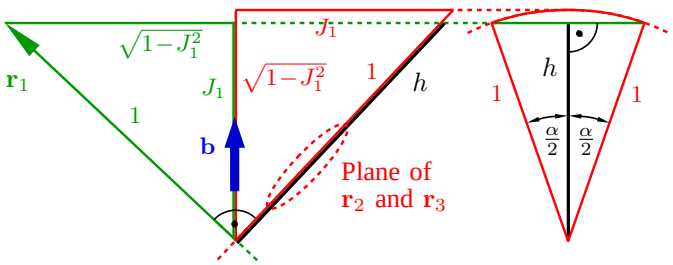

Fig. 3. Sketch of the transitional case in single-sided coil selection. Shown are the front view on the left-hand side and a lateral view to the right-hand side. For $\frac{1}{\sqrt{3}} < |\mathbf{r}_1^{\mathrm{T}}\mathbf{b}| \,/\, \|\mathbf{b}\| < \frac{1}{\sqrt{2}}$, the coil with orientation $\mathbf{r}_1$ may or may not have strongest coupling, depending on orientations $\mathbf{r}_2$ and $\mathbf{r}_3$.

$1 - \Pr(E_1 \;|\; \frac{1}{\sqrt{3}} < |J_1| < \frac{1}{\sqrt{2}}) = \frac{\alpha}{\pi/2}$. The intercept theorem yields $h = \frac{|J_1|}{\sqrt{1-J_1^2}}$. Clearly $\cos(\alpha/2) = h$, so

$$\Pr\left(E_1 \;\middle|\; \frac{1}{\sqrt{3}} < |J_1| < \frac{1}{\sqrt{2}}\right) = 1 - \frac{4}{\pi}\arccos\frac{|J_1|}{\sqrt{1-J_1^2}} \; .$$

From (12), $J_1 \sim \mathcal{U}(-1,1)$ so $f_{J_1}(J_1) = \frac{1}{2}$ there. $\Pr(E_m) = \frac{1}{3}$ due to symmetry. With marginalization and Bayes' rule,

$$\begin{aligned} f_J(J) &= \sum_{m=1}^{3} f_{J_m|E_m}(J|E_m) \cdot \underbrace{\Pr(E_m)}_{=1/3} = f_{J_1|E_1}(J|E_1) \\ &= \frac{\Pr(E_1|J_1 = J) f_{J_1}(J)}{\Pr(E_1)} = \frac{3}{2}\Pr(E_1|J_1 = J) \; . \end{aligned}$$

Using the results for $\Pr(E_1|J_1)$ leads to (14). The moments were obtained with a computer algebra system. □

Dipole-field case, single-sided beamforming: With uniformly random array orientation $\mathbf{R}$ (or $\mathbf{T}$), the link behaves like a 1×1 link of mutual inductance subject to

$$f_J(J) = \begin{cases} \frac{2}{\sqrt{3}}\frac{|J|}{\sqrt{4J^2-1}} & \frac{1}{2} \le |J| < 1 \\ 0 & \text{otherwise} \end{cases} \tag{15}$$

with moments $\mathrm{E}(J^2) = \frac{1}{2}$ and $\mathrm{E}(J^4) = \frac{3}{10}$.

Proof: For single-sided beamforming, $|J| = \frac{1}{2}\sqrt{1+3a^2}$ according to (10). Now, $a \sim \mathcal{U}(-1,1)$ by the argument of (12). The sign of the equivalent J is arbitrary, so let us assume an equivalent $J = \operatorname{sgn}(a) \cdot \frac{1}{2}\sqrt{1+3a^2}$ being realized by the beamformer, giving a one-to-one map $J = g(a)$. Therefore,

$$f_J(J) = f_a(g^{-1}(J)) \left|\frac{dg^{-1}(J)}{dJ}\right| = \frac{1}{2}\left|\frac{dg^{-1}(J)}{dJ}\right| \; .$$

Expanding g^{-1} and its derivative leads to the claim (15). □

Performance Comparison: The PDFs of J for all discussed setups are given in Figure 4. Distributions that could not be derived analytically were computed with Monte Carlo simulation. Figure 5 shows the CDFs of alignment efficiency J^2. Note the long tails of 1×1 links and the improvements from spatial diversity with coil arrays. All quantitative misalignment results are summarized in Table I.

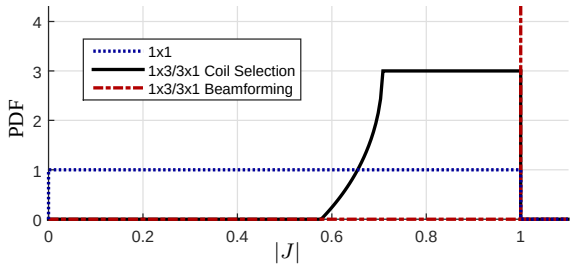

(a) Homogeneous-field case.

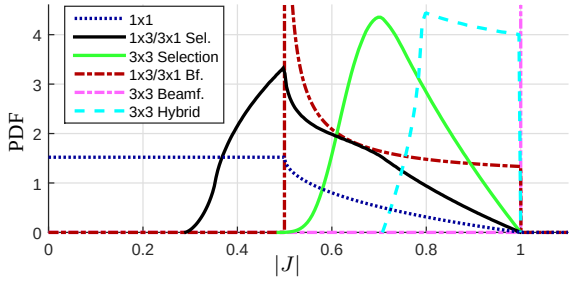

(b) Dipole-field case.

Fig. 4. Probability density functions of $|J|$ for random arrangement.

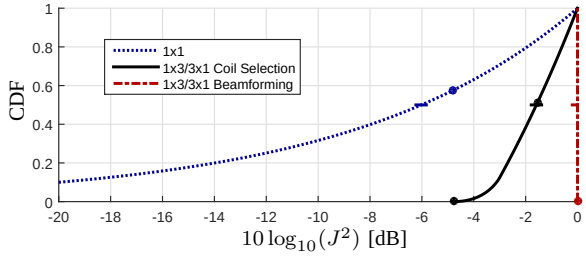

(a) Homogeneous-field case.

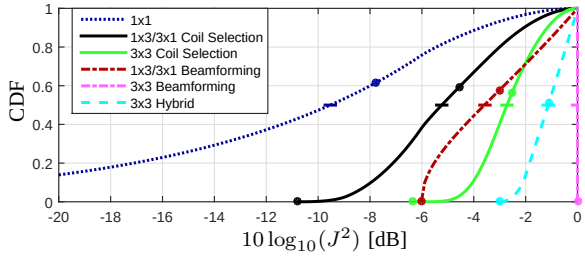

(b) Dipole-field case.

Fig. 5. CDFs of alignment efficiency of all introduced setups. Dots and dashes represent mean and median alignment efficiency, respectively. The 1×1 setups show particularly long tails: in the dipole-field case, the lower 10% are below -23.7 dB and the lowest 1% even below -43.7 dB. To obtain the CDF of load modulation alignment efficiency J^4, multiply dB-values by two.

Dipole-field case, ML range estimation: The 1×1 PDF (13) in (5) gives the PDF of mutual inductance given distance

$$f_{M|d}(M|d) = \frac{d^3}{K} \cdot f_J\Big(\frac{d^3}{K}M\Big) \ .$$

A noiseless mutual inductance measurement M_{meas} gives rise to ranging likelihood function $L(d) = f_{M|d}(M_{\text{meas}}|d)$ that is shown in Figure 6. The peak constitutes the maximum likelihood range estimate for unknown geometry

$$\hat{d}_{\text{ML}} = \arg\max_d L(d) = \sqrt[3]{\frac{K}{2M_{\text{meas}}}} \ ,$$

Case	Scheme	$M\times N$	$\min J^2$	$\mathrm{E}(J^2)$	$\mathrm{E}(J^4)$	$\min J^2$ [dB]	$\mathrm{E}(J^2)$ [dB]	$\mathrm{E}(J^4)$ [dB]
Hom. **b**	-	1×1	0	$1/3$	$1/5$	$-\infty$	-4.77	-6.99
	Select.	$3\times1^*$	$1/3$	.7009	.5185	-4.77	-1.54	-2.85
	Beamf.	$3\times1^*$	1	1	1	0	0	0
Dip. **b**	-	1×1	0	$1/6$	$3/50$	$-\infty$	-7.78	-12.2
	Select.	$3\times1^*$	$1/12$	.3504	.1556	-10.8	-4.55	-8.08
		3×3	.2302	.5586	.3319	-6.37	-2.53	-4.79
	Beamf.	$3\times1^*$	$1/4$	$1/2$	$3/10$	-6.02	-3.01	-5.23
		3×3	1	1	1	0	0	0
	Hybrid	3×3	$1/2$	.7757	.6170	-3.01	-1.10	-2.10

TABLE I
WORST-CASE AND EXPECTED ALIGNMENT EFFICIENCY FOR THE PRESENTED SCHEMES. $3\times1^*$ ROWS ALSO REPRESENT 1×3 RESULTS. $\mathrm{E}(J^4)$ IS THE EXPECTED ALIGNMENT EFFICIENCY OF LOAD MODULATION.

which corresponds to a $|J| = \frac{1}{2}$ case, e.g. coplanar coupling.

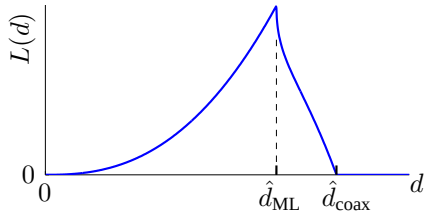

Fig. 6. Ranging likelihood function $L(d) = f_{M|d}(M_{\text{meas}}|d)$ for a mutual inductance measurement M_{meas} (assumed noiseless). $\hat{d}_{\text{ML}}$ is the maximum likelihood range estimate.

V. Circuit Aspects

When relating mutual inductance and communications performance, we must consider the underlying circuits in order to formulate a proper communications problem. We will briefly discuss the quintessence based on Figure 7.

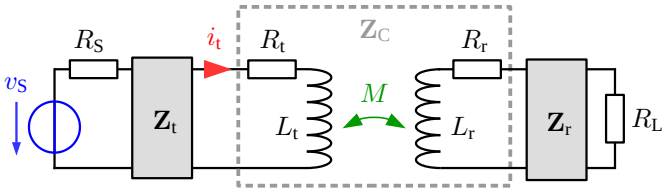

Fig. 7. General circuit model of a magneto-inductive 1×1 link.

R_{L} is the input resistance of a low-noise amplifier (LNA). The matching two-ports with impedance matrices $\mathbf{Z}_{\text{t}}$ and $\mathbf{Z}_{\text{r}}$ are typically used for power and noise matching, respectively. A sensible definition of TX-power P_{t} would be the active power flowing into $\mathbf{Z}_{\text{t}}$ and RX-power P_{r} the signal power over R_{L}. $|H|^2 = P_{\text{r}}/P_{\text{t}}$ is then the squared channel gain. Inductive coupling is expressed by the two-port

$$\mathbf{Z}_{\text{C}} = \begin{bmatrix} R_{\text{t}} + j\omega L_{\text{t}} & j\omega M \\ j\omega M & R_{\text{r}} + j\omega L_{\text{r}} \end{bmatrix} \ . \qquad (16)$$

The unilateral assumption $Z_{\text{C12}} = 0$ is reasonable in the weak-coupling regime, where coupling only negligibly affects coil

impedances and no detuning occurs. This is just the regime where $|H|^2 \propto M^2$ and consequently $|H|^2 \propto J^2$, which can be verified with basic circuit analysis. Misalignment efficiency results like Figure 5 thus directly *apply as attenuation* to SNR.

We denote by P_N the noise power over R_L due to LNA circuitry and thermal noise of RX coil serial resistance R_r. Thus, SNR $= |H|^2 P_\mathrm{t}/P_\mathrm{N}$ and achievable rate $B\log_2(1+\mathrm{SNR})$ over a narrow band B. For this communications model, the statistics of achievable rate for a 1×1 link of random arrangement are shown in Figure 8. Rates for M subject to our stochastic model (in particular, J sampled from (13)) are compared to rates where M was computed with numerical integration of the Neumann formula [7, Eq 7.22] for many random arrangements. The results show great agreement.

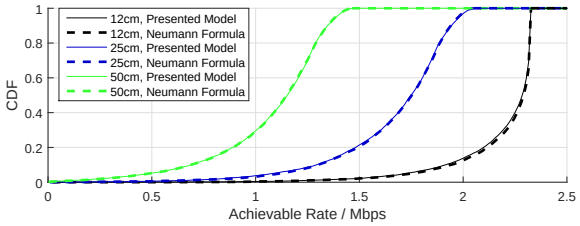

Fig. 8. Model comparison in terms of rate CDFs at different separations. Flat circular coils of 5 cm diameter were assumed. Reference values were computed with the Neumann double line integral. Parameter $N_\mathrm{t} = N_\mathrm{r} = 5$, $f_c = 25.4$ MHz, $B = 100$ kHz, $P_\mathrm{TX} = 1$ μW, LNA noise figure $= 15$ dB.

VI. Conclusion

We proposed a stochastic model for coil misalignment of magneto-inductive links, in order to dismiss aspects of arrangement geometry from the performance analysis of unaligned links. Under the assumption of uniformly random coil orientations we derived the PDF of mutual inductance for several practically relevant setups, involving single coils and coil arrays. Therewith, we studied the capabilities of beamforming and coil selection regarding mitigation of worst-case and average misalignment losses. The results serve as an alignment efficiency comparison of different array techniques, could aid the analysis of ergodic and outage capacity of MI links, and are valuable for MI localization and ranging.

Appendix A
Worst Case in 3×3 Coil Selection

The worst case J in 3×3 coil selection is the unique solution to the minimization problem

$$\zeta = \min_{\mathbf{J}=\mathbf{R}^\mathrm{T}\boldsymbol{\mathcal{E}}\mathbf{T}} \left(\max_{m,n} |J_{m,n}| \right)$$

over all arrangements $(\mathbf{e}, \mathbf{T}, \mathbf{R})$. There is a finite set of ζ-achieving matrices $\mathbf{J}$: neither changing the arbitrary antenna indexation order (swapping rows or columns in $\mathbf{J}$) nor reversing antenna orientations (applying sign flips to any rows or columns of $\mathbf{J}$) affects membership to the ζ-achieving set. Any ζ-achieving matrix $\mathbf{J}$ fulfills the following properties. (We verified them up to computational accuracy for several hundred numerical solutions with the global search algorithm with random initializations and all degrees of freedom. A rigorous argument could not be found.)

- *Six out of the nine elements* achieve $|J_{m,n}| = \zeta$, two have $|J_{m,n}| = \alpha$, and the last one $|J_{m,n}| = \beta$ with $\zeta > \alpha > \beta$.
- With a few sign flips and swaps to rows and columns (cf. above), any ζ-achieving $\mathbf{J}$ can be transformed to the ζ-achieving matrix $\mathbf{J}_*$ with eigenvalues $\{1, \frac{1}{2}, -\frac{1}{2}\}$ and

$$\mathbf{J}_* := \begin{bmatrix} \zeta & \zeta & \zeta \\ \zeta & \zeta & -\alpha \\ \zeta & -\alpha & \beta \end{bmatrix} . \qquad \text{(A.1)}$$

Comparing $\mathrm{tr}(\mathbf{J}_*)$, $-\det(\mathbf{J}_*)$, and $\mathrm{tr}(\mathbf{J}_*^2)$ due to eigenvalues and due to structure yields equations of numerical solution

$$\begin{aligned} 1 &= 2\zeta + \beta \\ \tfrac{1}{4} &= \zeta(\zeta+\alpha)^2 \\ \tfrac{3}{2} &= 6\zeta^2 + 2\alpha^2 + \beta^2 \end{aligned} \quad \Longrightarrow \quad \begin{aligned} \zeta &= 0.47978835338 \\ \alpha &= 0.24205864282 \\ \beta &= 0.04042329324 \ . \end{aligned}$$

Substitutions isolate $\left(24\zeta^3 - 8\zeta^2 - \zeta + 1\right)^2 - 16\zeta^3 = 0$. For $\mathbf{e} = [1,0,0]^\mathrm{T}$ ($\Longrightarrow$ $\boldsymbol{\mathcal{E}} = \mathrm{diag}(1, -\frac{1}{2}, -\frac{1}{2})$), a symmetric ζ-achieving arrangement is obtained by comparing an adapted EVD $\mathbf{J}_* = \mathbf{U} \cdot \mathrm{diag}(1, -\frac{1}{2}, -\frac{1}{2}) \cdot \mathrm{diag}(1,-1,1) \cdot \mathbf{U}^\mathrm{T}$ of (A.1) to (7), leading to $\mathbf{R} = \mathbf{U}^\mathrm{T}$ and $\mathbf{T} = \mathrm{diag}(1,-1,1) \cdot \mathbf{U}^\mathrm{T}$.

References

[1] S. Bi, C. Ho, and R. Zhang, "Wireless Powered Communication: Opportunities and Challenges," *Communications Magazine, IEEE*, vol. 53, no. 4, pp. 117–125, 2015.

[2] J. Jadidian and D. Katabi, "Magnetic MIMO: how to charge your phone in your pocket," in *Proceedings of the 20th annual international conference on Mobile computing and networking*. ACM, 2014.

[3] S. Kisseleff, I. Akyildiz, and W. Gerstacker, "Throughput of the magnetic induction based wireless underground sensor networks: Key optimization techniques," *Communications, IEEE Transactions on*, 2014.

[4] I. F. Akyildiz, P. Wang, and Z. Sun, "Realizing underwater communication through magnetic induction," *Communications Magazine, IEEE*, vol. 53, no. 11, 2015.

[5] B. Lenaerts and R. Puers, "Inductive powering of a freely moving system," *Sensors and Actuators A: Physical*, vol. 123, 2005.

[6] W. H. Ko, S. P. Liang, and C. D. Fung, "Design of radio-frequency powered coils for implant instruments," *Medical and Biological Engineering and Computing*, vol. 15, no. 6, pp. 634–640, 1977.

[7] D. J. Griffiths and R. College, *Introduction to Electrodynamics*. Prentice Hall, 1999, vol. 3.

[8] E. S. Hochmair, "System optimization for improved accuracy in transcutaneous signal and power transmission," *Biomedical Engineering, IEEE Transactions on*, no. 2, pp. 177–186, 1984.

[9] F. Flack, E. James, and D. Schlapp, "Mutual inductance of air-cored coils: Effect on design of radio-frequency coupled implants," *Medical and biological engineering*, vol. 9, no. 2, pp. 79–85, 1971.

[10] K. Fotopoulou and B. W. Flynn, "Wireless power transfer in loosely coupled links: Coil misalignment model," *Magnetics, IEEE Transactions on*, vol. 47, no. 2, pp. 416–430, 2011.

[11] M. Soma, D. C. Galbraith, and R. L. White, "Radio-frequency coils in implantable devices: misalignment analysis and design procedure," *Biomedical Engineering, IEEE Transactions on*, no. 4, 1987.

[12] Y. Huang, A. Nehorai, and G. Friedman, "Mutual coupling of two collocated orthogonally oriented circular thin-wire loops," *Antennas and Propagation, IEEE Transactions on*, vol. 51, no. 6, pp. 1307–1314, 2003.

[13] M. R. Andrews, P. P. Mitra *et al.*, "Tripling the capacity of wireless communications using electromagnetic polarization," *Nature*, vol. 409, no. 6818, pp. 316–318, 2001.

[14] G. Marsaglia, "Choosing a point from the surface of a sphere," *Ann. Math. Statist.*, vol. 43, no. 2, pp. 645–646, Mar. 1972.